A R&D software platform for shape and topology optimization using body-fitted meshes

Chiara Nardoni, David Danan, Chetra Mang, F Bordeu, Julien Cortial

A R&D software platform for shape and topology optimization using body-fitted meshes

C. Nardoni, D. Danan, C. Mang, F. Bordeu, J. Cortial

Abstract Topology optimization is devoted to the optimal design of structures: It aims at finding the best material distribution inside a working domain while fulfilling mechanical, geometrical and manufacturing specifications. Conceptually different from parametric or size optimization, topology optimization relies on a freeform approach enabling to search for the optimal design in a larger space of configurations and promoting disruptive design. The need for lighter and efficient structural solutions has made topology optimization a vigorous research field in both academic and industrial structural engineering communities. This contribution presents a Research and Development software platform for shape and topology optimization where the computational process is carried out in a level set framework combined with a body-fitted approach.

1 Introduction

Several shape and topology optimization methods have been proposed and are currently employed for structural design in commercial solutions (SIMP method, BESO method, level set method among them). Density-based optimization meth-

C. Nardoni
IRT SystemX, France, e-mail: chiara.nardoni@irt-systemx.fr

D. Danan
IRT SystemX, France, e-mail: david.danan@irt-systemx.fr

C. Mang
IRT SystemX, France, e-mail: chetra.mang@irt-systemx.fr

F. Bordeu
Safran Tech, France e-mail: felipe.bordeu@safrangroup.com

J. Cortial
Safran Tech, France e-mail: julien.cortial@safrangroup.com

ods, such as the widespread SIMP method, use as the design variable a density field which takes intermediate values between the material and the void densities. The fictious material densities are eventually penalized in order to enforce a binary material/void optimized design. In the present work we opt for level-set-based structural optimization in order to avoid the introduction and the treatment of ficticious material densities. The level set method relies on the classical sensitivity analysis from the shape optimization framework to compute a descent direction and advect the structural interface. The overall optimization process is driven by a gradient-type algorithm. In the present setting the level set method is coupled with a remeshing routine which enables the reconstruction of a body-fitted mesh at each step of the underlying optimization process, as proposed in [4, 8]. Since the structural interface is known explicitely at each step of the iterative procedure, the body-fitted approach simplifies the evaluation of the mechanical quantities of interest. Moreover, the computational mesh of the optimized design can be readily exported together with its finite element model for further validation analysis using a dedicated external software application.

In this work we handle two classical problems in structural optimization. First, in the static linear elasticity setting, we consider stress minimization problems. Avoiding stress concentration plays a paramount role in the design of reliable mechanical structures [2, 6, 13, 18, 20, 17, 21, 23]. In the present context we focus on the von Mises stress which is a key ingredient of most failure criteria. Second, we consider the problem of maximizing the first eigenfrequency of an elastic structure under a volume constraint. Vibration analysis is a also crucial assessment to avoid structural failure [16].

The proposed numerical examples are realized using PISCO, a Research and Development software platform devoted to topology optimization that is in active development at IRT SystemX[1]. Isovalue discretization, mesh adaptation and mesh displacement are performed by the remeshing tool `mmg3d`[2]. The finite element analyses are carried out using the industrial-grade solver `Code_Aster` [3].

2 Level set method for shape and topology optimization

This section introduces some basic notions about the level set method for shape and topology optimization. For more detailed surveys we refer to [1, 5, 22].

[1] https://www.irt-systemx.fr/project/top

[2] https://www.mmgtools.org/

[3] https://www.code-aster.org

2.1 Shape sensitivity analysis

Shape optimization aims at minimizing an objective function $J(\Omega)$ over a set O of admissible shapes. Typically the admissible shapes are constrained into a given design space D. In order to differentiate with respect to the domain and enforce optimality conditions, we refer here to the Hadamard's boundary variation method (see e.g. [1, 15]). Thus, variations of a given shape Ω are considered under the form:

$$\Omega_\theta = (I + \theta)(\Omega),$$

where $\theta : \mathbb{R}^d \mapsto \mathbb{R}^d$ is a 'small' diffeomorphism. Indeed, each admissible variation Ω_θ of Ω is parametrized in terms of a transformation of the form $I + \theta$, which remains 'close' to the identity. The admissible vector field θ is sought among the Banach space $W^{1,\infty}(\mathbb{R}^d, \mathbb{R}^d)$ of bounded and Lipschitz functions endowed with the norm:

$$||\theta||_{W^{1,\infty}(\mathbb{R}^d,\mathbb{R}^d)} := ||\theta||_{L^\infty(\mathbb{R}^d)^d} + ||\nabla\theta||_{L^\infty(\mathbb{R}^d)^{d\times d}}, \forall\theta \in W^{1,\infty}(\mathbb{R}^d, \mathbb{R}^d).$$

The shape derivative is then defined as follows.

Definition 1 A function $F(\Omega)$ of the domain is said to be *shape differentiable* at Ω if the mapping $\theta \mapsto F(\Omega_\theta)$, from $W^{1,\infty}(\mathbb{R}^d, \mathbb{R}^d)$ into $\mathbb{R}$, is Fréchet differentiable at $\theta = 0$. The associated Fréchet differential is denoted as $\theta \mapsto F'(\Omega)(\theta)$ and called the shape derivative of F; the following expansion then holds:

$$F(\Omega_\theta) = F(\Omega) + F'(\Omega)(\theta) + o(\theta), \text{ where } \frac{|o(\theta)|}{||\theta||_{W^{1,\infty}(\mathbb{R}^d,\mathbb{R}^d)}} \xrightarrow{\theta\to 0} 0.$$

We recall that for a large class of functions of the domain the shape derivative admits the following structure [1]:

$$\forall\theta \in W^{1,\infty}(\mathbb{R}^d, \mathbb{R}^d),\ F'(\Omega)(\theta) = \int_{\partial\Omega} v_\Omega(s)\theta n_{\partial\Omega}\, ds, \tag{1}$$

where $n_{\partial\Omega}$ is the outward normal to $\partial\Omega$ and v_Ω is a scalar field depending on F typically through a direct state and an adjoint state, both solutions of PDEs modeling the physical system of interest.

2.2 Level set method

2.2.1 Implicit parametrization of shapes

In the level set approach, the structural interface is represented as the 0 isovalue of a scalar function – the *level set function* – defined over the whole design space D. The implicit description allows to easily track the interface evolution and naturally

handles topology changes, as for example the merging of two interfaces. More precisely, a level set function of a shape $\Omega \subset D \subset \mathbb{R}^3$ is a scalar function $\phi : D \to \mathbb{R}$ enjoying the following properties

$$\begin{cases} \phi(x) < 0 \text{ si } x \in \Omega, \\ \phi(x) = 0 \text{ si } x \in \partial\Omega, \\ \phi(x) > 0 \text{ si } x \in {}^c\overline{\Omega}. \end{cases}$$

The level set function is typically initialized with the *signed distance function* d_Ω owing to the unitary gradient property:

$$|\nabla d_\Omega(x)| = 1,$$

which holds for all x where d_Ω is differentiable.

2.2.2 Optimization procedure

Starting from a given admissible shape Ω_0 and a function of the domain J, the shape derivative allows to select a descent direction for J. This procedure enables to produce a sequence of shapes $\Omega_{k\,\{k=0,\cdots\}}$ with decreasing values of J. At each iteration the domain is updated using the following advection equation

$$\frac{\partial \phi}{\partial t} + \theta_k |\nabla \phi| = 0 \text{ in } D, \tag{2}$$

where the vector field θ_k is a descent direction for J, set as

$$\theta_k = -w_{\Omega_k} n_{\partial\Omega_k}, \tag{3}$$

where w_{Ω_k} and $n_{\partial\Omega_k}$ are respectively a velocity field and the normal defined in (1). Thus, the new shape is defined implicitely by $\Omega_{k+1} = \{x \in D : \phi_{k+1}(x) < 0\}$.

2.2.3 Regularization of the descent direction

The field (1) is *only* rigorously defined on the interface $\partial\Omega$; it has to be extended to the whole domain to move the interface further than an infinitesimal distance. Moreover, the choice $\theta = -vn$ on $\partial\Omega$ can generate an irregular descent direction, unsuitable for numerical practice. To circumvent these difficulties, the literature suggests to *extend* and *regularize* the descent direction [9]. The general idea is to replace the optimal scalar product over $L^2(\partial\Omega)$ by a more regular one. In the present context the extended and regularized scalar field is defined as the unique solution $z \in H^1(\Omega)$ of the following variational problem

$$\forall w \in H^1(D),\ \alpha \int_\Omega \nabla z \cdot \nabla w \, dx + \int_{\partial\Omega} zw \, dx = \int_{\partial\Omega} v_{\partial\Omega} w \, ds, \tag{4}$$

where $\alpha > 0$ is a parameter tuning the intensity of the regularization.

3 Shape evolution using body-fitted meshes

At each step of the optimization procedure an unstructured mesh of the current shape is obtained by the explicit discretization of the 0 isovalue of the implicit domain ϕ_{k+1} [4, 8]. This routine allows to generate a tetrahedral mesh whose boundary fits the structural interface. This goal is achieved thanks to the following steps:

- The 0 isosurface of the level set function is explicitely discretized;
- The quality of the underlying mesh is improved by means of local remeshing operations driven by both geometrical and user requirements.

See Fig. 1 for an exemple of such a procedure. This method allows to dynamically track the evolution of the interface even when topology changes occur. Note that the isovalue discretization can be combined with classical metric-based adaptation routines, allowing the user to prescribe a spatially-varying desired mesh size.

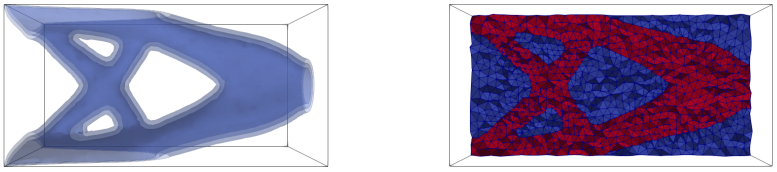

Fig. 1 Isovalues of the level-set function (left) and body-fitted mesh (right) of a given shape. The interior part of the shape is represented in red.

The above procedure permits the evaluation of the mechanical performances of the structure without falling back on the ersatz material approximation, which is currently used for level-set-based topology optimization in a fixed background mesh setting. This approximation can impact the accuracy of the finite element computation in some sensitive cases. For example, in the context of stress evaluation, in particularly when the volume fraction of the material part inside the design space is small, the residual stresses stored in the soft material can affect the measurement of global stress indicators as well as the local stresses near the interface [11]. A special attention must also be paid in the context of eigenfrequency optimization since the presence of a soft material [7] or a density-based approach [10] can modify the eigenfrequencies of the structure.

An alternative to conformal remeshing consists in keeping the computational support unchanged while enriching the finite element space in the vicinity of the interface with ad-hoc chosen basis functions (X-FEM-type methods [12, 19, 23]).

The main drawback of these methods is their intrusiveness making them difficult to couple with existing physical solvers.

4 Stress-based optimization

Let $\Omega \subset \mathbb{R}^3$ be a shape such that $\partial\Omega = \Gamma_D \cup \Gamma_N \cup \Gamma$. Let u_Ω be the displacement field solution of the following linear elasticity problem

$$\begin{cases} -\mathrm{div}(\sigma(u_\Omega)) = 0 & \text{in } \Omega, \\ \sigma(u_\Omega) \cdot n = g & \text{on } \Gamma_N, \\ \sigma(u_\Omega) \cdot n = 0 & \text{on } \Gamma, \\ u_\Omega = 0 & \text{on } \Gamma_D. \end{cases} \tag{5}$$

where $\varepsilon(u) = \frac{1}{2}(\nabla u + \nabla u^T)$ is the linearized strain tensor and σ is the stress tensor obeying to the following Hooke's law with Lamé parameters λ, μ:

$$\sigma(u) = 2\mu\varepsilon(u) + \lambda\ \mathrm{tr}(\varepsilon(u))I.$$

Let us denote by $\sigma_{vm}(u)$ the Von Mises equivalent stress associated to $\sigma(u)$. Since stress measurements are intrinsically of local nature, a typical stress constraint over a region Ω translates into the following non differentiable form

$$\max_{x \in \Omega(x)} \sigma_{vm}(x) \leq \bar{\sigma}_{vm}, \forall x \in \Omega. \tag{6}$$

From a numerical point of view, incorporating such a condition at each stress evaluation point leads to an unacceptably large number of constraints that further increases with the refinement of the underlying computational mesh. In order to overcome these difficulties constraints aggregation techniques can be considered. A popular choice [2, 21] consists in regularizing the criterion (6) by penalizing the following integral functional:

$$J(\Omega) = \left(\int_\Omega j_\alpha(\sigma(u_\Omega))\, dx \right)^{\frac{1}{\alpha}} = \left(\int_\Omega \sigma_{vm}^\alpha(u_\Omega)\, dx \right)^{\frac{1}{\alpha}}, \tag{7}$$

where $j_\alpha = \sigma_{vm}^\alpha$ and $\alpha \geq 1$ is a scalar parameter. By a classical calculation (see for example [2]) the functional (7) is shape differentiable. In the present context the descent direction θ is sought in the space

$$\Theta_{ad} = \{\theta = 0 \text{ on } \Gamma_N \cup \Gamma_D\}.$$

Thus the shape derivative of (7) reads

$$\forall \theta \in \Theta_{ad}, J'(\Omega)(\theta) = \frac{1}{\alpha} J(\Omega)^{1-\alpha} \int_\Gamma (\sigma_{vm}^\alpha(u_\Omega) + \sigma(u_\Omega) : \varepsilon(p_\Omega))\theta \cdot n\, ds. \tag{8}$$

The *adjoint state* p_Ω is solution of the following problem

$$\begin{cases} -\mathrm{div}(\sigma(p_\Omega)) = \mathrm{div}(Aj'_\alpha(\sigma(u_\Omega)) & \text{in } \Omega, \\ \sigma(p_\Omega)\cdot n = Aj'_\alpha(\sigma(u_\Omega))\cdot n & \text{on } \Gamma\cup\Gamma_N, \\ p_\Omega = 0 & \text{on } \Gamma_D, \end{cases} \tag{9}$$

where j'_α denotes the derivative of j_α with respect to σ.

Remark 1 As noted in [18], increasing the exponent α can lead to overly large values of the integrand in (8). To avoid degrading the numerical accuracy, one can consider an alternative, mathematically equivalent formulation such that the integrand is defined as:

$$j_\alpha = \left(\frac{\sigma_{vm}}{\bar{\sigma}}\right)^\alpha, \tag{10}$$

where $\bar{\sigma}$ is a normalization parameter.

5 k-th eigenfrequency maximization

In this section we focus on a criterion that requires a modal search analysis. Let $\Omega \subset \mathbb{R}^3$ be a shape such that $\partial\Omega = \Gamma_D \cup \Gamma$. The eigenmodes and eigenfrequencies of Ω are determined by solving the following problem

$$\begin{cases} -\mathrm{div}(\sigma(u_\Omega)) = \omega^2\rho u_\Omega & \text{in } \Omega, \\ u_\Omega = 0 & \text{on } \Gamma_D, \\ \sigma(u_\Omega)n = 0 & \text{on } \Gamma, \end{cases} \tag{11}$$

where ρ denotes the material density. Note that (11) admits a countable set of solutions $(\omega_k, u_k)_{k\in\mathbb{N}}$. When the positive values ω_k are sorted such that $\omega_k < \omega_{k+1}$, $\forall k$, then u_k is called the k-th eigenvector or eigenmode. The quantity

$$f_k = \frac{\omega_k}{2\pi}$$

is called the k-th eigenfrequency of the structure. Moreover each eigenmode is normalized as follows

$$\int_\Omega \rho|u_k|^2 dx = 1, \ \forall k. \tag{12}$$

In order to maximize the k-th eigenfrequency we consider the minimization of following functional of the domain

$$J_k(\Omega) = -\omega_k^2. \tag{13}$$

A classical computation (see for example [3]) shows that if the eigenvalue associated to the k-th eigenmode is simple, then (13) is shape differentiable and the shape derivative reads

$$\forall \theta \in \Theta_{ad}, J'(\Omega)(\theta) = \int_{\Gamma} (\omega_k^2 \rho |u_{k\Omega}|^2 - \sigma(u_{k\Omega}) : \varepsilon(u_{k\Omega}))\theta \cdot n ds, \qquad (14)$$

where Θ_{ad} is the set

$$\Theta_{ad} = \{\theta = 0 \text{ on } \Gamma_D\}.$$

Note that the above problem is self-adjoint, meaning that the evaluation of the shape derivative does not require the computation of an adjoint state. Note also that functional (13) extends without difficulty to the optimization of a continuously differentiable function of eigenfrequencies.

6 Numerical implementation

PISCO includes the following components:

- An algorithmic toolbox specialized in the treatment of level sets
- A generic interface to finite element solvers
- Algorithms for the resolution of constrained optimization problems
- Physical and geometrical optimization criteria
- An interface to the remeshing tool `mmg3d`

The components devoted to the physical analysis computations and the constrained optimization algorithms are implemented in a generic fashion in dedicated modules. These components are linked to the topology optimization problems and criteria in a non-intrusive way. The non-intrusiveness of the implementation is proved by the coupling with several external physical solvers such as `Code_Aster` and `FreeFem++`. In the present context, all physical evaluations are performed using the finite element solver `Code_Aster`, developed at EDF France. The choice of `Code_Aster` is motivated by the large range of availables physics and by the richness of the available post-processing routines.

The numerical optimization algorithm handles the balancing between the minimization of the objective and the non-violation of the constraints. Popular penalization methods such as the Augmented Lagrangian reformulate a constrained optimization problem into a sequence of unconstrained optimization problems by incorporating the constraints as penalizations of the objective function. In the present context, we rely on a gradient-flow algorithm designed to decrease both the value of the objective function and the violation of the constraints [14].

6.1 Overview of the numerical algorithm

As far as the numerical setting is concerned, the initial shape Ω_0 is supplied through its signed distance function ϕ_0, e.g. as a $\mathbb{P}^1$ piecewise affine function on the mesh of the design space D. A remeshing procedure is employed to compute a new mesh

$\mathcal{T}_0$ of the design space in which the structural interface is explicitely discretized. The mesh $\mathcal{T}_0$ contains naturally a computational mesh of the shape Ω_0 as a subdomain. The complete numerical procedure allows to generate a sequence of meshes $\mathcal{T}_{k\,\{k=0,\cdots\}}$. Each mesh $\mathcal{T}_k$ contains a submesh corresponding to a body-fitted discretization of the shape Ω_k. At each iteration k the domain evolution is achieved numerically by the following steps:

1. Computation of the signed distance function to the shape Ω_k on the vertices of the mesh $\mathcal{T}_k$;
2. Evaluation of the direct and the adjoint physical states on the computational mesh of the shape Ω_k;
3. Evaluation of the objective function and constraints values on the shape Ω_k;
4. Evaluation of physical and geometrical sensitivities on the vertices of the structural interface;
5. Combination of physical and geometrical sensitivities and resolution of (4) on $\mathcal{T}_k$ in order to select a descent direction θ_k;
6. Selection of a pseudo time t_k and resolution of the advection equation (2) on the mesh $\mathcal{T}_k$ to get a $\mathbb{P}^1$ piecewise affine function of the domain ϕ_{k+1};
7. Check geometrical conditions for the acceptance of the implicit shape ϕ_{k+1};
8. When all the geometrical requirements are fulfilled, remesh $\mathcal{T}_k$ and generate a new mesh $\mathcal{T}_{k+1}$ to fit the structural interface of the implicit domain ϕ_{k+1}.

The algorithms ends whenever a maximum number of design steps is reached or when the merit function measuring jointly the decrease of the objective function and the non-violation of the constraints fails to decrease.

Remark 2 The variational formulation (4) is solved using $\mathbb{P}^1$ finite elements. The level set transport equation (2) is solved by a spatial first-order numerical scheme based on the method of characteristics. The variational formulations associated to the evaluation of values and sensitivities of each optimization criterion are discretized using linear or high-order elements, depending on user requirements.

6.2 Stress sensitivity evaluation on the structural interface

In stress-based optimization problems the integrand appearing in (8) has to be evaluated on the structural interface. To achieve this goal the sensitivity field in (8) is extrapolated from the stress evaluation points to the structural interface nodes. The nodal extrapolation is achieved by a least-squares approach based on a finite element interpolation. Eventually, for a given node, the nodal value is computed by weighting the values over the elements sharing the node. We consider the following smoothing function inside each finite element

$$\hat{s}(x) = \sum_{i=1}^{n} N_i(x)\hat{s}_i(x), \tag{15}$$

where $\hat{s}_i$ are the nodal unknown values, N_i the shape function at node i in the considered finite element. For each finite element, these unknowns are defined as the minimizer of a discrete functional

$$\chi(\tilde{\sigma}) \equiv \sum_{k=1}^{n_{GP}} (s(\xi_k) - \tilde{s}(\xi_k))^2 = \sum_{k=1}^{n_{GP}} (s(\xi_k) - \sum_{i=1}^{n} \tilde{s}_i N_i(\xi_k))^2, \tag{16}$$

where n_{GP} and $\xi_{k\,\{k=1,\cdots,n_{GP}\}}$ are respectively the number and the coordinates of the evaluation points (i.e. the Gauss integration points) inside the element. Under the assumption $n < n_{GP}$, the minimization of (16) implies the resolution of the following linear system (hereafter written in matrix form)

$$\hat{s} = M^{-1} P s. \tag{17}$$

Note that the matrices $P \in \mathbb{R}^{n \times n_{GP}}$, $P_{ik} = N_i(\xi_k)$ and $M = PP^T \in \mathbb{R}^{n \times n}$ can be pre-calculated in the reference finite element, resulting in a very efficient extrapolation procedure. Note that the above general procedure can be used for the extrapolation of stress-based quantities (equivalent stresses, elastic density energy for exemple) from Gauss integration points to mesh nodes. In stress-based optimization problems, the described procedure is used to extrapolate the stress-based integrand appearing (8) to the structural interface nodes.

Remark 3 An alternative approach consists in replacing the discrete functional (16) by the following functional

$$\bar{\chi}(\tilde{s}) \equiv \int_e (s - \tilde{s})^2 dx = \int_e (s - \sum_{i}^{n} N_i \tilde{s}_i)^2 dx. \tag{18}$$

where e denotes any element. In this case the matrices M et P need to be evaluated on each finite element making the extrapolation procedure more expensive.

7 Numerical results

This section presents the numerical examples.

7.1 Mininum stress design of an L-shaped beam

Let us consider an L-shaped design domain D with a bounding box of size 2 m $\times$ 1 m $\times$ 2 m. The beam is clamped on the plane $z = 2$ m and submitted to a vertical load $g = (0, 0, 10)$ kN on a small circular region of radius $r = 0.1$ m on the plane $x = 2$ m, as represented in Fig. 2–left. The Young modulus is equal to 210 GPa and the Poisson ratio equals 0.3. The Dirichlet and Neumann boundaries are sourrounded by

two non-optimisable regions, as represented in Fig. 2–right. Here the linear elastic system (5) is solved using $\mathbb{P}^2$ finite elements. A 5-point Gauss integration rule is used in each tetrahedral finite element.

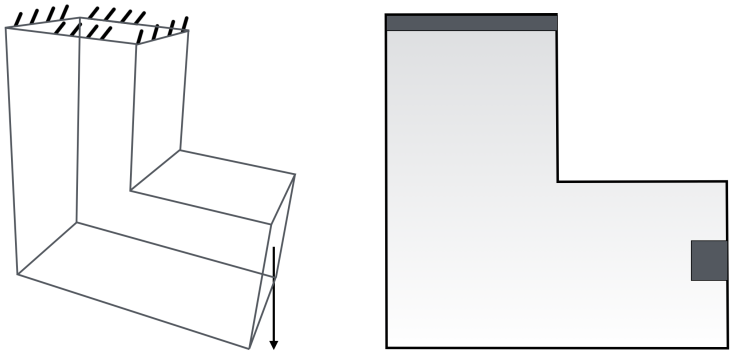

Fig. 2 Boundary conditions for the L-beam test case (left). Design space in light grey and non-optimizable regions in dark grey (right).

The goal is to minimise the global Von Mises indicator (7) under a volume constraint. The target volume is set to 0.7 m^3. For the value $\alpha = 2$ in the objective function (7), the optimized design is represented in Fig. 3 and for $\alpha = 12$ the optimized design is represented in Fig. 4. Note that for a small value of the parameter α ($\alpha = 2$ here) the optimized design is reminicent of one obtained when minimizing compliance. As the parameter α increases ($\alpha = 12$ here) the obtained design is modified in order to avoid stress concentration regions (in the vicinity of the sharp angle here), which are not captured using a compliance-type criterion.

7.2 Maximum eigenfrequency design of a cantilever beam

Let us consider a design space of size $2\,\mathrm{m} \times 0.5\,\mathrm{m} \times 1\,\mathrm{m}$. The structure is clamped on the right plane $x = 0\,\mathrm{m}$ and includes a concentrated tip mass localized at point $(2\,\mathrm{m}, 0\,\mathrm{m}, 0.5\,\mathrm{m})$, as represented in Fig. 5.

The material density of the structure is set to $0.42\,\mathrm{kg.m^{-3}}$. The point mass is set to 420 kg. The Young modulus is fixed to 32000 Pa and the Poisson coefficient to 0.3. The goal is to maximize the first eigenfrequency of the structure under a volume constraint. The target volume equals $\frac{1}{2}V_0$ with V_0 the volume of the full design space. The optimized design achieved after 90 iterations is represented in Fig. 6.

Remark 4 Since the level set approach enables the generation of arbitrary topologies, some intermediate shapes can exhibit several disconnected components. In this case, all components connecting the supports of boundary conditions constitute the

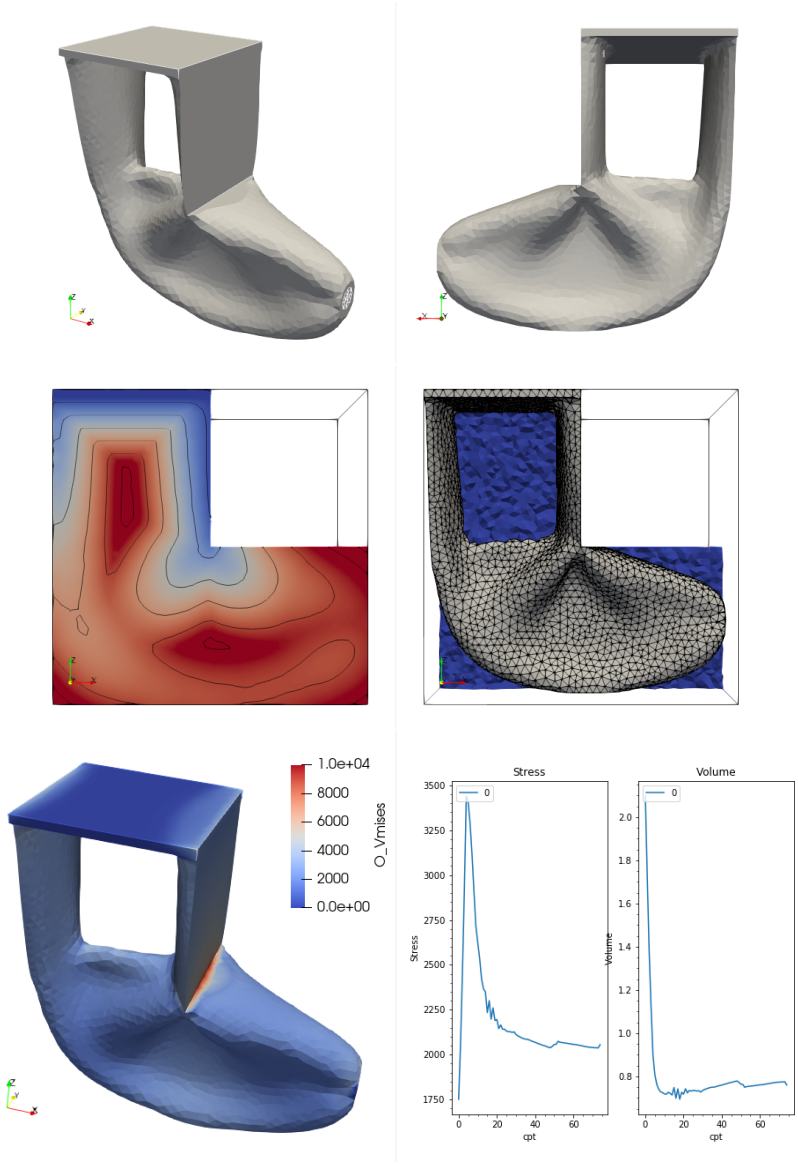

Fig. 3 Two views of the optimized design with $\alpha = 2$ (top). Level set function and body-fitted mesh of the optimized design (middle). Von Mises stress and convergence history for the L-beam test case with $\alpha = 2$ (bottom).

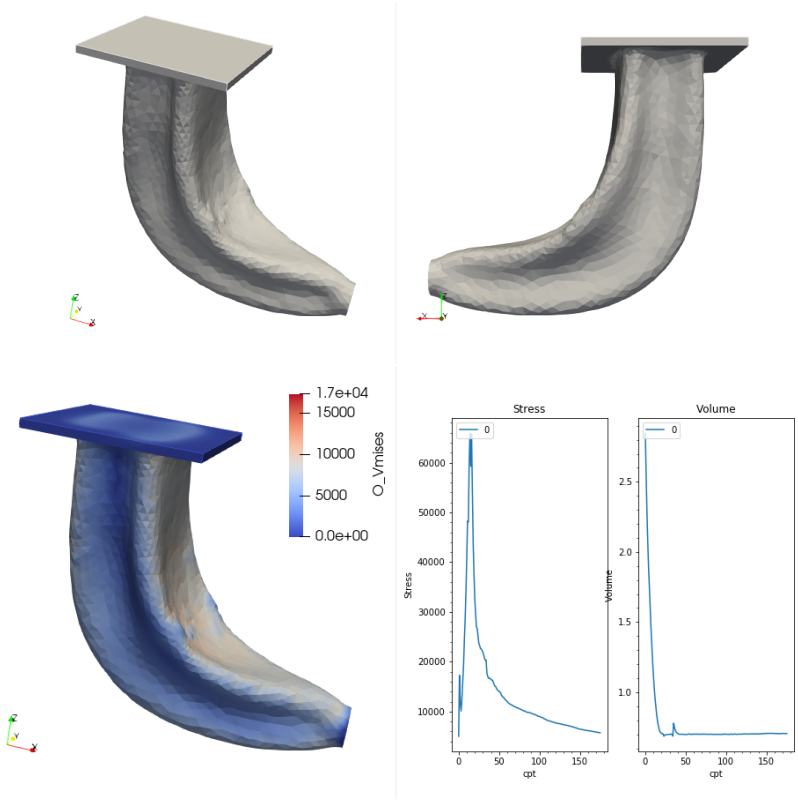

Fig. 4 Two views of the optimized design with $\alpha = 12$ (top). Von Mises stress and convergence history for the L-beam test case with $\alpha = 12$ (bottom).

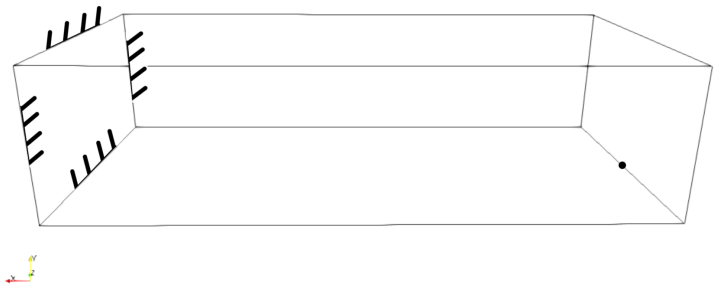

Fig. 5 Boundary conditions for the cantilever test case: clamped face (on the left) and point mass (on the right).

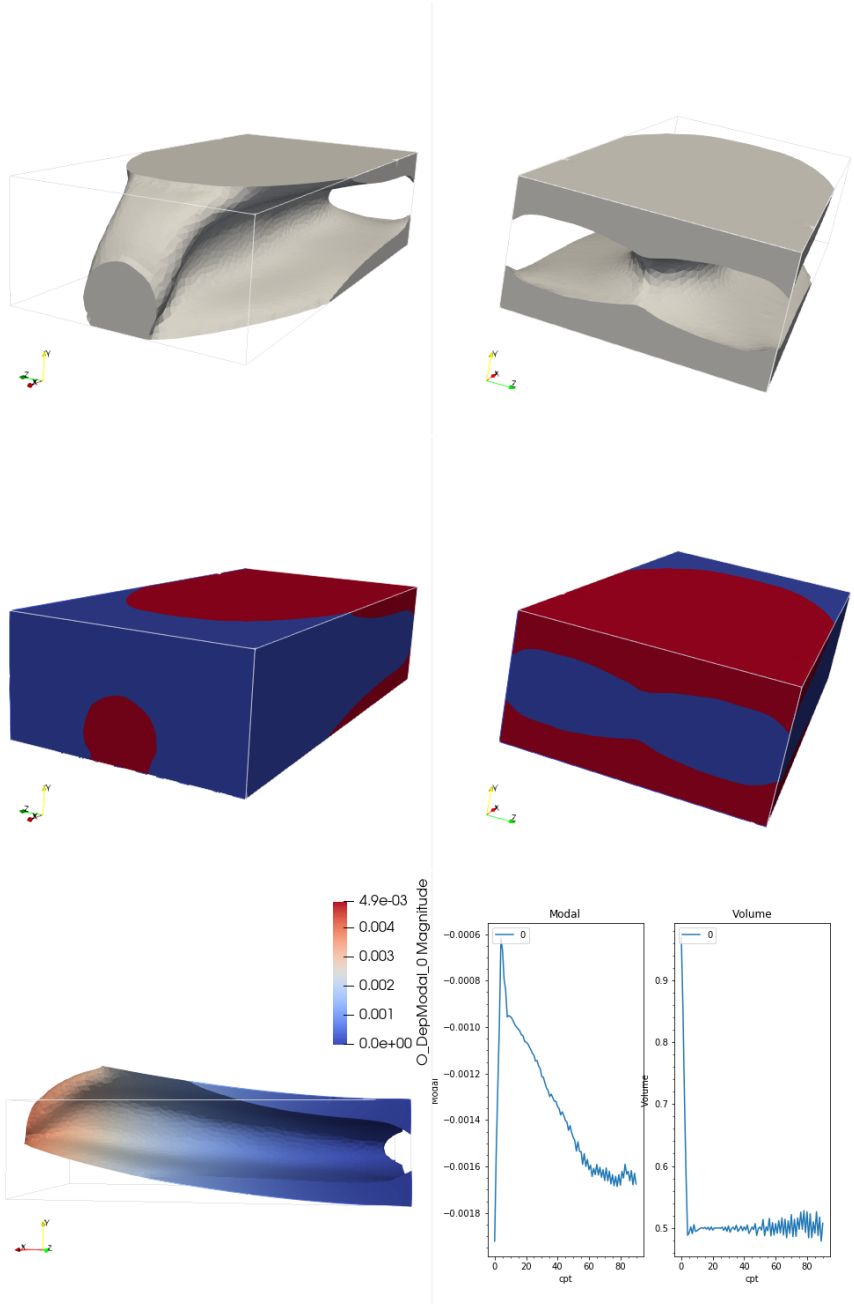

Fig. 6 Two views of the optimized design (top). Optimized design inside the design space. First eigenmode amplified by a factor of 70 and convergence history for the test case described in Section 7.2 (bottom).

actual, useful shape. The others are spurious components that are detected and removed before remeshing to avoid the existence of artificial rigid body modes during the eigenvalues analysis.

8 Conclusions

A computational solution for shape and topology optimization using level sets and body-fitted meshes has been discussed and illustrated on some classical albeit challenging optimization problems.

Acknowledgements

This research work has been carried out in the framework of IRT SystemX, Paris-Saclay, France, and therefore granted with public funds within the scope of "Programme d'Investissements d'Avenir". The authors would like to sincerely thank the industrial and academic partners of TOP project and the mmg team for the ongoing development of the mmg software package.

References

1. G. Allaire, *Conception optimale de structures*, (Springer Verlag, Heidelberg, 2006).
2. G. Allaire, F. Jouve, *Minimum stress optimal design with the level set method*, Engineering Analysis with Boundary Elements, 32(11), 909–918, Elsevier, 2008.
3. G. Allaire, F. Jouve, *A level-set method for vibration and multiple loads structural optimization*, Computer Methods in Applied Mechanics and Engineering, 194(30-33), 3269–3290, Elsevier, 2005.
4. G. Allaire, Ch. Dapogny, P. Frey, *A mesh evolution algorithm based on the level set method for geometry and topology optimization*, Structural and Multidisciplinary Optimization, 711–715, Springer, 2013.
5. G. Allaire, Ch. Dapogny, F. Jouve, *Shape and topology optimization*, to appear in Handbook of Numerical Analysis 22, Geometric PDES, (2020).
6. S. Amstutz, A. Novotny, *Topological optimization of structures subject to von Mises stress constraints*, Structural and Multidisciplinary Optimization, 41(3), 407–420, Springer, 2010.
7. A. Dalklint, M. Wallin, D. Tortorelli, *Eigenfrequency constrained topology optimization of finite strain hyperelastic structures*, Structural and Multidisciplinary Optimization, 1–18, Springer, 2020.
8. Ch. Dapogny, C. Dobrzynski, P. Frey, *Three-dimensional adaptive domain remeshing, implicit domain meshing, and applications to free and moving boundary problems*, J. Comput. Phys, 262, 358–378, 2014.
9. F. De Gournay, *Velocity extension for the level-set method and multiple eigenvalues in shape optimization*, SIAM Journal on Control and Optimization, 45(1), SIAM, 2006.
10. J. Du, N. Olhoff, *Topological design of freely vibrating continuum structures for maximum values of simple and multiple eigenfrequencies and frequency gaps*, Structural and Multidisciplinary Optimization, 34(2), 91–110, Springer, 2007.
11. P. Dunning, A. Kim, G. Mullineux, *Investigation and improvement of sensitivity computation using the area-fraction weighted fixed grid FEM and structural optimization*, Finite Elements in Analysis and Design, 47(8), 933–941, Elsevier, 2011.
12. P. Duysinx, L. Van Miegroet, T. Jacobs, C. Fleury, *Generalized shape optimization using X-FEM and level set methods*, IUTAM Symposium on Topological Design Optimization of Structures, Machines and Materials, 23–32, Springer, 2006.
13. P. Duysinx, L. Van Miegroet, E. Lemaire, O. Brüls, M. Bruyneel, *Topology and generalized shape optimization: Why stress constraints are so important?*, International Journal for Simulation and Multidisciplinary Design Optimization, 2(4), 253–258, EDP Sciences, 2008.
14. F. Feppon, G. Allaire, C. Dapogny, *Null space gradient flows for constrained optimization with applications to shape optimization*, ESAIM: Control, Optimisation and Calculus of Variations, 26(90), EDP Sciences, 2020.
15. A. Henrot, M. Pierre, *Variation et optimisation de formes, une analyse géométrique*, (Springer, Heidelberg, 2005).
16. Z. Kang, J. He, L. Shi, Z. Miao, *A method using successive iteration of analysis and design for large-scale topology optimization considering eigenfrequencies*, Computer Methods in Applied Mechanics and Engineering, 362, Elsevier, 2020.
17. O. Giraldo-Londoño, G.H. Paulino, *A unified approach for topology optimization with local stress constraints considering various failure criteria: Von Mises, Drucker–Prager, Tresca, Mohr–Coulomb, Bresler–Pister and Willam–Warnke*, Proceedings of the Royal Society A, 476(2238), The Royal Society Publishing, 2020.
18. E. Holmberg, B. Torstenfelt, A. Klarbring, *Stress constrained topology optimization*, Structural and Multidisciplinary Optimization, 48(1), 33–47, Springer, 2013.
19. N. Moës, J. Dolbow, T. Belytschko, *A finite element method for crack growth without remeshing*, International journal for numerical methods in engineering, 46(1), 131–150, Wiley Online Library, 1999.
20. C. Le, J. Norato, T. Bruns, C. Ha, D. Tortorelli, *Stress-based topology optimization for continua*, Structural and Multidisciplinary Optimization, 41(4), 605–620, Springer, 2010.

21. R. Picelli, S. Townsend, C. Brampton, J. Norato, A. Kim, *Stress-based shape and topology optimization with the level set method*, Computer Methods in Applied Mechanics and Engineering, 329, 1–23, Elsevier, 2018.
22. N. van Dijk, K. Maute, M. Langelaar, F. Van Keulen, *Level-set methods for structural topology optimization: A review*, Structural and Multidisciplinary Optimization, 48(3), 437–472, Springer, 2013.
23. L. Van Miegroet, P. Duysinx, *Stress concentration minimization of 2D filets using X-FEM and level set description*, Structural and Multidisciplinary Optimization, 33(4-5), 425–438, Springer, 2007.
24. Q. Xia, T. Shi, M. Wang, *A level set based method for topology optimization of continuum structures with stress constraint*, 6th China-Japan-Korea Joint Symposium on Optimization of Structural and Mechanical Systems, Kyoto, Japan, 2010.